The thermal behavior and pyrolysis mechanism of polyimide gas separation membrane

Qinxu Li[1,a], Bo Chen[2,a], Songyuan Yao[1,a], Chao Sang[1], Lu Lu[3], Shilong Dong[1], Hui Cao[1], Zhihao Si[1,], Peiyong Qin[1,*]*

[1]National Energy R&D Center for Biorefinery, College of Life Science and Technology, Beijing University of Chemical Technology, Beijing 100029, PR China

[2]Systems, Power and Energy Research Division, James Watts School of Engineering, College of Science and Engineering, James Watt South, University of Glasgow, Glasgow G128QQ, UK

[3]Paris Curie Engineer School, Beijing University of Chemical Technology, Beijing 100029, PR China

[a]These authors contributed equally to this paper.

*Corresponding author

*(Z. Si) E-mail zhsi@mail.buct.edu.cn.

*(P. Qin) E-mail qinpeiyong@tsinghua.org.cn.

Contents

Supplementary Figures

Figures

S1. Publication number related to 'Polyimide' and 'Membranes' in the literatures during 2003 to 2023.

S2. The heating program of the tube furnace.

S3. (a) XRD spectrum and (b) Raman spectrum of PI membrane.

S4. N 1s spectra of PI membrane.

S5. SEM image of PI membrane.

Tables

S1. Kissinger-Akahira-Sunose, Flynn-Wall-Ozawa and Starink methods formulas.

S2. All parameters used in the listed formulas and their units.

S3. Kinetic reaction models used in this work.

S4. Elemental composition of PI membrane analyzed by XPS and elemental analysis.

S5. The characteristic parameters of TGA-DTG curves of PI membrane under varying heating rate.

S6. Pyrolysis products of PI membrane at 600 °C.

S7. The activation energy and linear corelation coefficients at different conversion rates calculated by FWO, KAS and Starink method.

S8. Thermodynamic parameters of at heating rate of 10 °C min^{-1}.

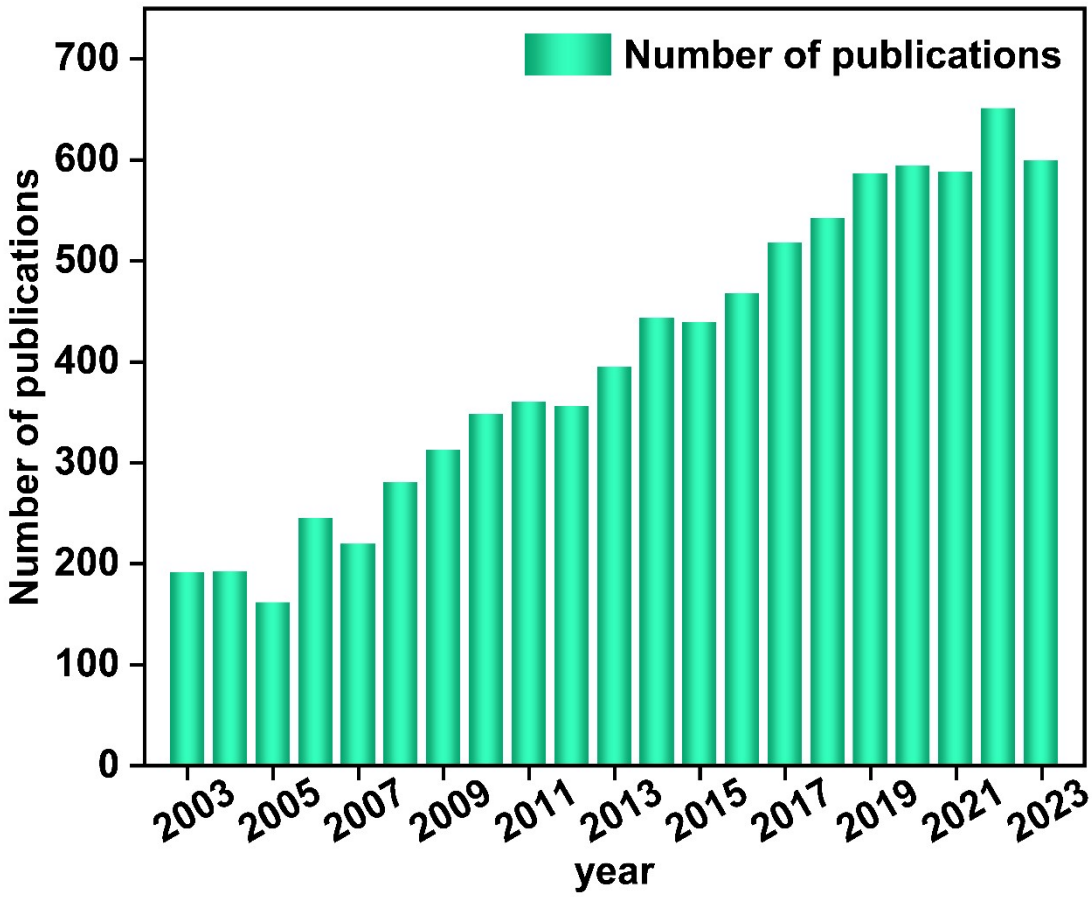

Figure S1. Publication number related to 'Polyimide' and 'Membranes' in the literatures during 2003 to 2023.

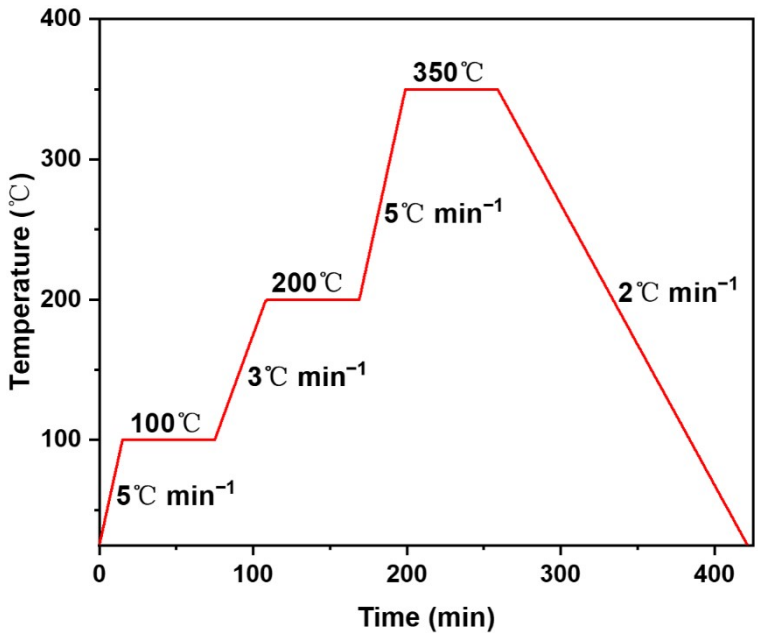

Figure S2. The heating program of the tube furnace.

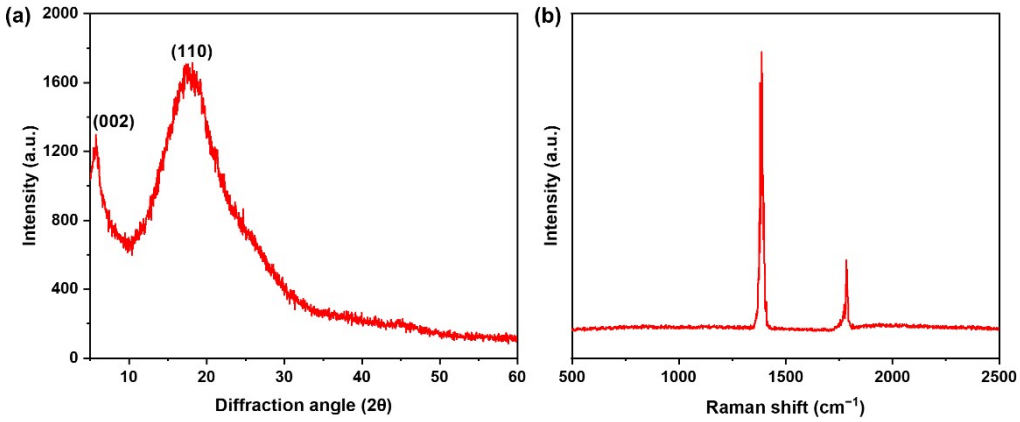

Figure S3. (a) XRD pattern and (b) Raman spectrum of PI membrane.

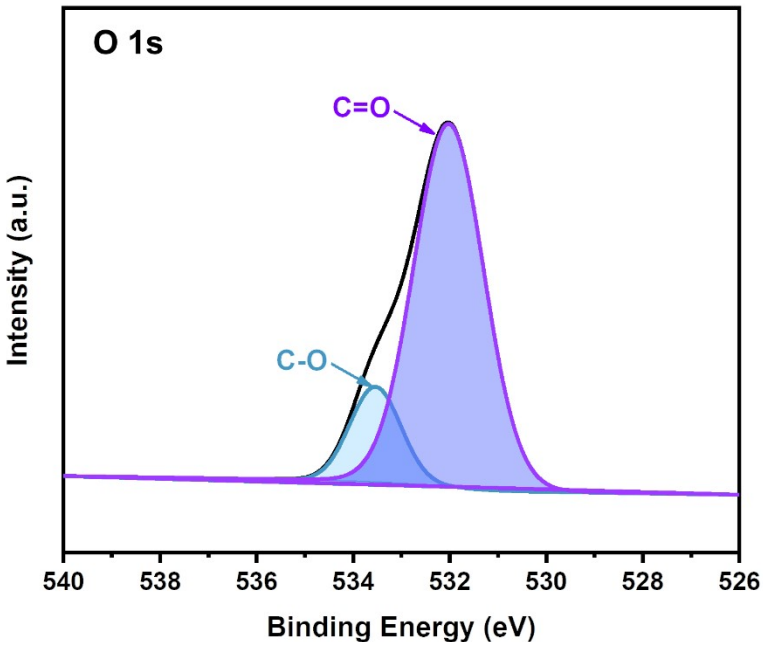

Figure S4. N 1s spectra of PI membrane.

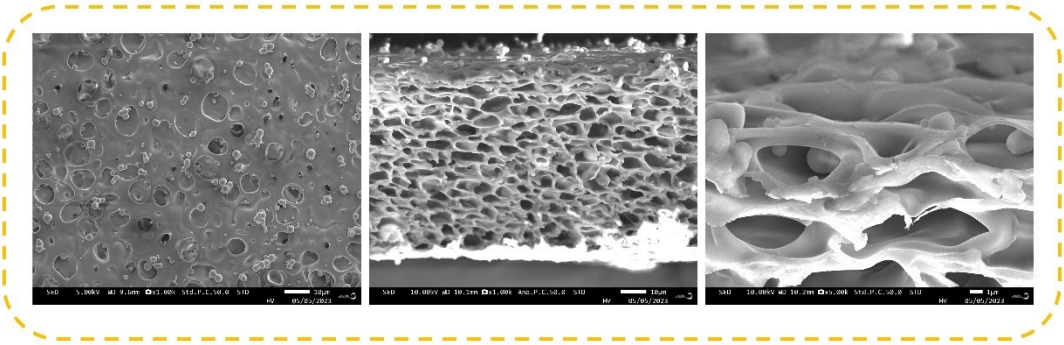

Figure S5. SEM image of PI membrane.

Table S1. Kissinger-Akahira-Sunose, Flynn-Wall-Ozawa and Starink methods formulas.

Eq. No.	Method	Expressions	Plots	Slope value
(1)	Kissinger-Akahira-Sunose	$\ln\left(\frac{\beta}{T^2}\right) = \ln\left(\frac{AR}{E_a g(\alpha y)}\right) - \frac{-E_a}{RT}$	$\ln\left(\frac{\beta}{T^2}\right)$ versus $1/T$	E_a/R
(2)	Flynn-Wall-Ozawa	$\ln\beta = \left(\frac{\ln AE_a}{Rg\alpha}\right) - 5.335 - \frac{1.0516E_a}{RT}$	$\ln\beta$ versus $1/T$	$-1.0516E_a/R$
(3)	Starink	$\ln\left(\frac{\beta}{T^{1.92}}\right) = \ln\left(\frac{AR^{0.92}}{g(\alpha)E^{0.92}}\right) - 0.312 - \frac{1.0008E_a}{RT}$	$\ln\left(\frac{\beta}{T^{1.92}}\right)$ versus $1/T$	$-1.0008E_a/R$

Table S2. All parameters used in the listed formulas and their units.

Parameters	Definition	value
$d\alpha/dt$	Rate of degradation	
$k(T)$	Temperature-dependent rate constant	
$f(\alpha)$	Reaction model	
m_0	Initial mass	
m_t	Actual mass	
m_f	Final mass	
$\beta=dT/dt$	Heating rate	
$T_{0.5}$	The temperature when $\alpha = 0.5$.	
$G(\alpha)$	The integral of kinetic reaction model (**Table S3**)[1-5]	
y	Conversion rate	
β	Heating rate	
T	Thermodynamic temperature (K)	
	Maximum decomposition temperature (°C)	
Ea	Activation energy (kJ mol^{-1})	
A	Pre-exponential factor (S^{-1})	
R	Gas constant (J mol^{-1} K^{-1})	8.314

ΔH	Enthalpy change (kJ mol^{-1})	
ΔS	Entropy change (kJ mol^{-1})	
ΔG	Gibbs free energy (kJ mol^{-1})	
k_B	Boltzmann constant (J K^{-1})	1.38×10^{-23}
h	Planck constant	6.626×10^{-34}

Table S3. Kinetic reaction models used in this work.

Kinetic reaction model	symbol	$f(\alpha)$	$G(\alpha)$
Chemical reaction models			
First order (Random nucleation and nuclei growth: n=1)	F_1	$1-\alpha$	$-\ln(1-\alpha)$
Second order (Random nucleation with two nuclei on the individual particle: n=2)	F_2	$(1-\alpha)^2$	$(1-\alpha)^{-1}-1$
Third order (Random nucleation with two nuclei on the individual particle: n=3)	F_3	$(1-\alpha)^3$	$0.5\left[(1-\alpha)^{-2}-1\right]$
Diffusion models			
One-dimensional diffusion	D_1	0.5α	α^2
Two-dimensional diffusion (Valensi)	D_2	$[-\ln(1-\alpha)]^{-1}$	$(1-\alpha)\ln(1-\alpha)+\alpha$
Three-dimensional diffusion (Jander)	D_3	$3\sqrt[3]{1-\alpha}/\left\{2\left[(1-\alpha)^{-1/3}-1\right]\right\}$	$[1-\sqrt[3]{1-\alpha}]^2$
Three-dimensional diffusion (Ginstling-Brounshtein)	D_4	$1.5\left[(1-\alpha)^{-1/3}-1\right]$	$[1-(2\alpha/3)]-(1-\alpha)^{2/3}$
Contraction models			
Phase-boundary-controlled reaction (contracting disk)	R_1	1	α
Phase-boundary-controlled reaction (contracting cylinder)	R_2	$2\sqrt{1-\alpha}$	$1-\sqrt{1-\alpha}$
Phase-boundary-controlled reaction (contracting sphere)	R_3	$3(1-\alpha)^{2/3}$	$1-\sqrt[3]{1-\alpha}$
Nucleation models			
Avrami-Eroféev (Random nucleation and nuclei growth: n=1/2, m=2)	A_2	$2(1-\alpha)\sqrt{-\ln(1-\alpha)}$	$\sqrt{-\ln(1-\alpha)}$
Avrami-Eroféev (Random nucleation and nuclei growth: n=1/3, m=3)	A_3	$3(1-\alpha)[-\ln(1-\alpha)]^{2/3}$	$\sqrt[3]{-\ln(1-\alpha)}$
Power law	P_2	$2\alpha^{1/2}$	$\alpha^{1/2}$
Power law	P_3	$3\alpha^{2/3}$	$\alpha^{1/3}$
Power law	P_4	$4\alpha^{3/4}$	$\alpha^{1/4}$

Table S4. Elemental composition of PI membrane analyzed by XPS and elemental analysis.

Sample type	XPS elemental composition (atom. %)			Elemental analysis (wt. %)			
	C	O	N	C	O	N	H
PI	74.64	7.19	18.17	68.52	21.92	6.72	2.84

Table S5. The characteristic parameters of TGA-DTG curves of PI membrane under varying heating rate.

Parameters	Heating rates (°C min^{-1})			
	5	10	20	30
T_m (°C)	575.5	588.5	598.1	603.9
R_{max} (% min^{-1})	3.08	6.69	13.32	19.44
M_f (%)	52.07	49.65	50.07	49.92

Table S6. Pyrolysis products of PI membrane at 600 °C.

Compound Name	RT	Area%	Molecular Formula	Compound Structure
Carbon dioxide	1.64	47.65	CO_2	
Oxygen	1.19	16.67	O_2	
Phenol	7.00	6.8	C_6H_6O	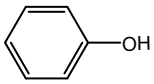
Aniline	6.41	4.29	C_6H_7N	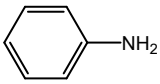
Benzonitrile	6.54	3.84	C_7H_5N	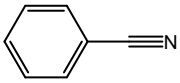
Benzene	2.50	3.34	C_6H_6	
4-Phenoxyaniline	16.89	1.43	$C_{12}H_{11}NO$	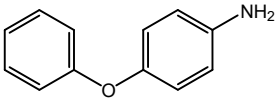
Dibenzofuran	14.16	1.03	$C_{12}H_8O$	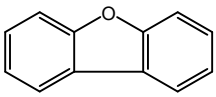

1,4-Dicyanobenzene	10.96	0.91	$C_8H_4N_2$	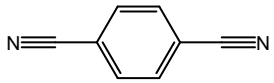
1,3-Dicyanobenzene	10.96	0.91	$C_8H_4N_2$	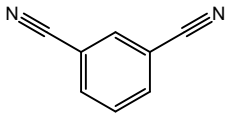
Phenyl isocyanate	6.11	0.88	C_7H_5NO	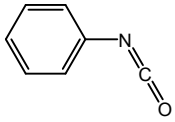
2-Cyanobenzoic acid	13.83	0.88	$C_8H_5NO_2$	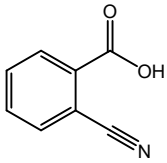
Phthalimide	13.83	0.88	$C_8H_5NO_2$	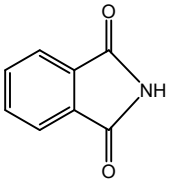
2-Phenylisoindole-1,3-dione	19.85	0.79	$C_{14}H_9NO_2$	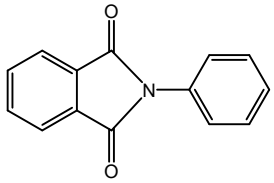
p-Aminophenol	11.47	0.57	C_6H_7NO	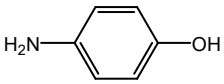
2-Dibenzofuranamine	18.51	0.56	$C_{12}H_9NO$	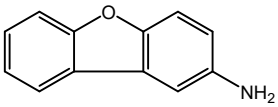
4,4'-Diaminodiphenyl ether	20.73	0.55	$C_{12}H_{12}N_2O$	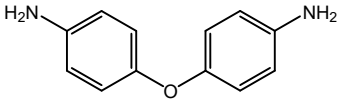
Diphenyl ether	12.60	0.53	$C_{12}H_{10}O$	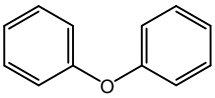
2-(4-Hydroxyphenyl)isoindoline-1,3-dione	23.25	0.32	$C_{14}H_9NO_3$	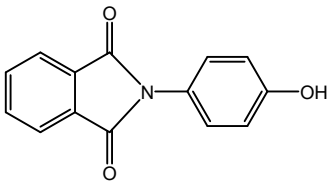

Table S7. The activation energy and linear corelation coefficients at different conversion rates calculated by FWO, KAS and Starink method.

α	FWO		KAS		Starink	
	E_a (kJ mol^{-1})	R^2	E_a (kJ mol^{-1})	R^2	E_a (kJ mol^{-1})	R^2
0.1	283.7	0.976	284.7	0.974	285.0	0.974
0.2	307.9	0.985	309.8	0.983	310.1	0.983
0.3	318.3	0.987	320.6	0.986	320.9	0.986
0.4	325.6	0.989	328.1	0.988	328.4	0.988
0.5	328.1	0.991	330.6	0.990	330.9	0.990
0.6	325.6	1	327.8	0.993	328.2	0.993
0.7	308.3	0.999	309.4	0.999	309.7	0.999
0.8	231.5	0.981	232.3	0.979	232.7	0.979
0.9	130.5	0.901	131.8	0.876	132.4	0.878
Average	284.4	0.979	286.1	0.974	286.5	0.974

Table S8. Thermodynamic parameters of at heating rate of 10 °C min^{-1}.

α	FWO				KAS				Starink			
	A (s^{-1})	ΔH (kJ mol^{-1})	ΔG (kJ mol^{-1})	ΔS (kJ $mol^{-1}\cdot K^{-1}$)	A (s^{-1})	ΔH (kJ mol^{-1})	ΔG (kJ mol^{-1})	ΔS (kJ $mol^{-1}\cdot K^{-1}$)	A (s^{-1})	ΔH (kJ mol^{-1})	ΔG (kJ mol^{-1})	ΔS (kJ $mol^{-1}\cdot K^{-1}$)
0.1	7.26×10^{16}	276.9	224.2	61.1	8.38×10^{16}	277871.2	224.2	62.3	8.75×10^{16}	278.2	224.2	62.7
0.2	2.31×10^{18}	300.9	223.6	89.7	3.03×10^{18}	302812.4	223.6	92.0	3.16×10^{18}	303.1	223.6	92.3
0.3	1.02×10^{19}	311.2	223.4	101.9	1.42×10^{19}	313524.3	223.3	104.7	1.48×10^{19}	313.8	223.3	105.0
0.4	2.89×10^{19}	318.5	223.2	110.5	4.13×10^{19}	320955.3	223.2	113.5	4.31×10^{19}	321.3	223.2	113.8
0.5	4.13×10^{19}	320.9	223.2	113.4	5.90×10^{19}	323390.4	223.1	116.4	6.16×10^{19}	323.7	223.1	116.7
0.6	2.89×10^{19}	318.3	223.2	110.4	3.96×10^{19}	320515.6	223.2	113.0	4.19×10^{19}	320.9	223.2	113.4
0.7	2.45×10^{18}	300.9	223.6	89.7	2.86×10^{18}	302005	223.6	91.0	2.99×10^{18}	302.3	223.6	91.4
0.8	4.06×10^{13}	223.9	225.7	-2.1	4.55×10^{13}	224686.4	225.6	-1.1	4.82×10^{13}	225.1	225.6	-0.6
0.9	1.72×10^{7}	122.3	229.8	-124.7	2.09×10^{7}	123617.7	229.7	-123.1	2.28×10^{7}	124.2	229.7	-122.4

References

1 S. Kumagai, T. Hosaka, T. Kameda and T. Yoshioka, Pyrolysis and hydrolysis behaviors during steam pyrolysis of polyimide, *J. Anal. Appl. Pyrol.,* 2016, 120, 75-81.

2 Y. Wen, Z. Shi, S. Wang, W. Mu, P. G. Jönsson and W. Yang, Pyrolysis of raw and anaerobically digested organic fractions of municipal solid waste: Kinetics, thermodynamics, and product characterization, *Chem. Eng. J.,* 2021, 415, 129064.

3 D. Irmak Aslan, P. Parthasarathy, J. L. Goldfarb and S. Ceylan, Pyrolysis reaction models of waste tires: Application of Master-Plots method for energy conversion via devolatilization, *Waste Manage.,* 2017, 68, 405-411.

4 S. Vyazovkin, A. K. Burnham, J. M. Criado, L. A. Pérez-Maqueda, C. Popescu and N. Sbirrazzuoli, ICTAC Kinetics Committee recommendations for performing kinetic computations on thermal analysis data, *Thermochim. Acta,* 2011, 520(1-2), 1-19.

5 S. Majoni and A. Chaparadza, Thermal degradation kinetic study of polystyrene/organophosphate composite, *Thermochim. Acta,* 2018, 662, 8-15.